RSC Advances

PAPER

View Article Online
View Journal | View Issue

Cite this: *RSC Adv.*, 2018, **8**, 41439

Efficient photoelectrochemical water oxidation using a TiO_2 nanosphere-decorated $BiVO_4$ heterojunction photoanode †

Wenchao Jiang, Yi Jiang,* Jing Tong, Qian Zhang, Siyuan Li, Haili Tong and Lixin Xia*

Constructing heterojunctions by coupling dissimilar semiconductors is a promising approach to boost charge separation and charge transfer in photoelectrochemical (PEC) water splitting. In this work, we fabricated a highly efficient $TiO_2/BiVO_4$ heterojunction photoanode for PEC water oxidation *via* a simple hydrothermal method. The resulting heterojunction photoanodes show enhanced PEC performance compared to the bare $BiVO_4$ due to the simultaneous improvements in charge separation and charge transfer. Under simulated sunlight illumination (AM 1.5G, 100 mW cm^{-2}), a high photocurrent of 3.3 mA cm^{-2} was obtained at 1.23 V (*vs.* the reversible hydrogen electrode (RHE)) in a neutral solution, which exceeds those attained by the previously reported $TiO_2/BiVO_4$ heterojunctions. When a molecular Co–cubane catalyst was immobilized onto the electrode, the performance of the $TiO_2/BiVO_4$ heterojunction photoanode can be further improved, achieving a higher photocurrent density of 4.6 mA cm^{-2} at 1.23 V, an almost three-fold enhancement over that of the bare $BiVO_4$. These results engender a promising route to designing an efficient photoelectrode for PEC water splitting.

Received 2nd November 2018
Accepted 3rd December 2018

DOI: 10.1039/c8ra09072f

rsc.li/rsc-advances

Introduction

With gradual, increasing consumption resulting in the depletion of traditional fossil fuels, new forms of energy are being investigated. Sunlight has attracted more interest as it is the most abundant renewable energy source.[1–3] Solar energy, a new type of renewable energy, has the advantages of being a clean and inexhaustible source of energy and is attracting research interest. Splitting water into hydrogen and oxygen using sunlight, *via* photoelectrochemical (PEC) devices, is a promising method of converting and storing solar energy as a chemical fuel.[2–5] To date, an enormous effort has been invested in this field, however, the development of a highly efficient PEC water splitting cell for solar-to-hydrogen fuel conversion remains a challenge.[6,7] And the PEC water splitting using semiconductors has received increasing attention, owing to the semiconductors have excellent light absorption characteristics, for example, bismuth vanadate ($BiVO_4$) and TiO_2. $BiVO_4$ has appropriate band-edge position (2.4 eV) and a wide range of absorption of sunlight.[8,9] However, the unmodified $BiVO_4$ has significant electron–hole recombination and poor water oxidation kinetics.[10] Various strategies have been implemented to address these restrictions, such as nanostructured control,[11] elemental doping,[12,13] loading cocatalysts such as Co–Pi,[14–16] FeOOH[17] and NiOOH,[10,18] construction of heterojunction,[19,20] and plasmonic enhancement.[21–23]

In principle, constructing heterojunctions is the most effective and direct way to promote the efficiency of charge-separation in photoelectrodes. Many studies have investigated $BiVO_4$-based heterojunction photoanodes, such as $WO_3/BiVO_4$,[24–26] $TiO_2/BiVO_4$,[27–29] *etc.* These composites have been demonstrated to have higher PEC performance compared to $BiVO_4$. TiO_2 has been intensively studied as a candidate photoanode due to its favourable band-edge positions, high resistance to photocorrosion, physical and chemical stability, nontoxicity and low cost.[30,31] Recent studies have reported an improvement in PEC water oxidation using $TiO_2/BiVO_4$ heterojunctions.[32] However, a high photocurrent density for this heterojunction electrode is scarce.

In this study, a facile hydrothermal method using modified nanoporous $BiVO_4$ photoanodes with TiO_2 nanospheres was proposed to develop $TiO_2/BiVO_4$ heterojunction photoanodes. The $BiVO_4$ layers in this photoanode absorb sunlight and the TiO_2 nanospheres facilitate the separation and transmission of the photogenerated charge in $BiVO_4$. The shift of TiO_2 and $BiVO_4$ interfacial Fermi levels result in the formation of an n–n junction at the interface,[33] promoting electron–hole separation. The proposed $TiO_2/BiVO_4$ heterojunction photoanodes had good PEC performance. A high photocurrent density of 3.3 mA cm^{-2} was achieved at 1.23 V, compared to a reversible hydrogen electrode (RHE) in a neutral electrolyte, which is much higher

College of Chemistry, Liaoning University, Shenyang 110036, Liaoning, China. E-mail: jiangyi@lnu.edu.cn; lixinxia@lnu.edu.cn

† Electronic supplementary information (ESI) available. See DOI: 10.1039/c8ra09072f

than that of $BiVO_4$ and exceeds other $TiO_2/BiVO_4$ heterojunctions reported. To further optimise the kinetics of surface water oxidation of photoanodes, a molecular Co–cubane water oxidation catalyst (WOC) was immobilized on the electrode and an extremely high photocurrent density of 4.6 mA cm^{-2} was achieved at 1.23 V *vs.* RHE.

Experimental section

Fabricate of the $BiVO_4$ photoanode

The $BiVO_4$ electrodes were prepared by using an electrodeposition process as reported.[10] Briefly, the electrodeposited solution was prepared as follow: 2.91 g $Bi(NO_3)_3 \cdot 5H_2O$ (99.0%, AR) and 9.96 g KI (99.0%, AR) were dissolved in 150 mL deionized water respectively before its pH was adjusted to 1.7 by adding HNO_3, then this solution was mixed with 20 mL of absolute ethanol contained 1.49 g *p*-benzoquinone (99%) by stirring for a few minutes vigorously. A three-electrode cell was used for electrodeposition, with an FTO as the working electrode, an Ag/AgCl (3.5 M KCl) reference, and a platinum counter electrode. A CHI660 was used for electrodeposition studies. Deposition was carried out potentiostatically at −0.1 V *vs.* Ag/AgCl for 3 min at 30 °C (equivalent to passing a total charge of 0.45C cm^{-2}). All prepared films were rinsed by deionised water and blow-dried with nitrogen. 10 mL of a dimethyl sulfoxide (DMSO, AR) solution containing 1.06 g vanadyl acetylacetonate ($VO(acac)_2$ 98%) was placed on the BiOI electrode. Then the BiOI electrodes were annealed at 450 °C (ramping rate = 2 °C min^{-1}) for 2 h. After annealing, the as deposited film was converted to crystalline $BiVO_4$ and amorphous V_2O_5, and pure $BiVO_4$ was obtained by dissolving the V_2O_5 in 1 M NaOH under stirring for several minutes.

Fabricate of the $TiO_2/BiVO_4$ photoanode

The $TiO_2/BiVO_4$ electrode was developed using a hydrothermal method. The TiO_2 nanospheres were formed using a hydrolysis reaction. 1 mL of $TiCl_4$ solution was added to 50 mL deionized water, and centrifuged for 5 min at 10 000 rpm until the suspended precipitate was spun down into a pellet. The supernatant was removed and precipitate resuspended in deionized water. The TiO_2 aqueous solution was subjected to ultrasonic treatment to promote the dispersion of TiO_2 nanospheres throughout the solution. A $BiVO_4$ electrode was immersed into the TiO_2 aqueous solution for 10 min (10 min-$TiO_2/BiVO_4$), 30 min (30 min-$TiO_2/BiVO_4$) and 60 min (60 min-$TiO_2/BiVO_4$) at 60 °C. Finally, the electrode was washed using deionized water and then calcined at 500 °C for 2 h in air (2 °C min^{-1}).

Development of a TiO_2 photoanode

A TiO_2 electrode was prepared using a spin-coating method. TiO_2 was deposited onto the FTO using spin coating at 1000 rpm for 20 s. The spin coating solution was the previously described solution in Section 2. After spin coating, the samples were annealed at 500 °C for 2 h with a temperature increase of 2 °C min^{-1}.

Synthesis of Co–cubane catalyst

The Co-catalyst was synthesised as below: $Co(NO_3)_2 \cdot 6H_2O$ (2.90 g, 10 mmol) and $CH_3COONa \cdot 3H_2O$ (2.70 g, 20 mmol) added in 30 mL methanol and heated to refluxing temperature, then 4-cyanopyridine (10 mmol) was added to the reaction mixture. 30% hydrogen peroxide (5 mL) was slowly added into the reaction mixture, which was held at reflux for a further 4 h. The reaction mixture was cooled and concentrated in a rotary evaporator, and the aqueous layer was separated by adding CH_2Cl_2. The light pink aqueous layer was discarded, and the CH_2Cl_2 layer was dried using anhydrous Na_2SO_4. An olive-green compound precipitated out on addition of petroleum ether. Fig S1† is the structure of the Co–cubane. Fig S2† is the ^{1}H-NMR of the catalyst. ^{1}H-NMR (500 MHz, CD3OD): 8.65 (d, 8H), 7.62 (d, 8H), 2.2 (d, 12H).

Preparation of the Co–cubane/$TiO_2/BiVO_4$ photoanode

The catalyst solution is prepared by dissolving the Co–cubane catalyst into solution (CH_3OH/CH_2Cl_2/Nafion mixture (7 : 2.5 : 0.5, v/v)) at a concentration of 1 mM. A 10 μL of the cobalt catalyst was then cast onto the surface of the $TiO_2/BiVO_4$ electrode and dried at room temperature.

Photoelectrochemical measurements

The PEC performance of the $BiVO_4$ and $TiO_2/BiVO_4$ electrodes were tested in 0.1 M PBS solution and AM 1.5 G simulated sunlight illumination (100 mW cm^{-2}). The active surface area of the $BiVO_4$ and $TiO_2/BiVO_4$ heterojunctions were 1 cm^2. A CHI660 was used for electrochemical PEC measurements which contained samples as the working electrode, an Ag/AgCl (3.5 M KCl) reference and a platinum counter electrode. EIS measurements was carried out at 0.6 V *versus* Ag/AgCl. Mott–Schottky measurements were performed under dark conditions, in the potential range −0.6 to +1.0 V *versus* Ag/AgCl with 500 Hz. All the potentials are presented against the reversible hydrogen electrode (RHE), and the conversion between the Ag/AgCl and RHE was performed using the equation:

$$E_{RHE} = E_{Ag/AgCl} + 0.059\ pH + 0.197\ V$$

Incident photon-to-current efficiency (IPCE) at each wavelength was determined using illumination from a 300 W Xe arc lamp and neutral density filters, to imitate the light from the sun. Monochromatic light was produced using an Oriel Cornerstone 130 monochromator with a 10 nm bandpass, and the output was measured using a photodiode detector. IPCE was measured at 0.6 V *vs.* RHE using the same three-electrode setup described above for the photocurrent measurements.

$$IPCE = \frac{J \times \lambda}{P_{light}} \times 100\%$$

where: J is the photocurrent density, λ is the incident light wavelength and P_{light} is the measured irradiance.

The applied bias photon-to-current efficiency (ABPE) was calculated from a *J–V* curve, where: J is the photocurrent density,

V_{bias} is the applied bias and P_{in} is the incident illumination power density (AM 1.5 G, 100 mW cm^{-2}):

$$\mathrm{ABPE} = \frac{J \times (1.23 - V_{bias})}{P_{in}} \times 100\%$$

The η_{tr} was calculated using the equation:

$$\eta_{tr} = J_{water}/J_{Na_2SO_3}$$

where: J_{water} is the $TiO_2/BiVO_4$ electrode photocurrent density in 0.1 M PBS, $J_{Na_2SO_3}$ is the $TiO_2/BiVO_4$ electrode photocurrent density in 0.1 M PBS containing 0.1 M Na_2SO_3.

Results and discussion

A porous $BiVO_4$ was produced using the previously reported method.[10] Fig. 1a shows the microstructure of the porous $BiVO_4$; the significant voids can be seen clearly. The porous structure of the $BiVO_4$ enables sites for the TiO_2 nanospheres to attach. TiO_2 nanospheres, with a range of diameter size 200 to 500 nm (illustrated by DLS in Fig S3†) were attached onto the $BiVO_4$ electrodes using a hydrothermal method. The SEMs of $TiO_2/BiVO_4$ electrodes with different hydrothermal times are shown in Fig. 1b–d, which show that the TiO_2 nanospheres were attached onto the $BiVO_4$ successfully and the quantity of TiO_2 nanospheres increased with immersed time. The elemental mapping results shown in Fig. 1e–h suggest the existence of O, Ti, Bi, and V elements, indicating a uniform distribution of TiO_2 nanospheres across the structure.

The crystalline structures of the FTO, $BiVO_4$ and $TiO_2/BiVO_4$ samples were characterised using X-ray diffraction (XRD) patterns, as shown in Fig S4,† further confirming that TiO_2 attached to the porous $BiVO_4$ and that the crystalline structures of TiO_2 are anatase.

In order to gain more insight into $TiO_2/BiVO_4$ heterojunctions, X-ray photoelectron spectroscopy (XPS) characterisation was performed, which showed signals from Ti, O, Bi and V elements (Fig. S5†). The HR-XPS spectra of the $TiO_2/BiVO_4$ are shown in Fig. 2. Two binding energy peaks for a typical Bi element in $BiVO_4$ occurred at 158.9 and 164.2 eV, corresponding to the Bi 4f7/2 and Bi 4f5/2, suggesting that Bi is present as Bi^{3+} (Fig. 2a).[34] The binding energies of the vanadium(v) peaks were centred at 516.5 and 524.5 eV, corresponding to V 2p3/2 and V 2p1/2 orbits, respectively, characteristic of the presence of the V^{5+} oxidation state (Fig. 2b).[35] Two peaks for Ti 2p at 458.7 and 465.7 eV were assigned to Ti 2p3/2 and Ti 2p1/2, respectively, suggesting a Ti^{4+} oxidation state (Fig. 2c).[36] The peak at binding energy of 529.8 eV in Fig. 2d, indicates that oxygen was present as surface lattice oxygen and free oxygen.[37]

The PEC performance of the $BiVO_4$ and $TiO_2/BiVO_4$ was measured using a three electrode system which included the proposed electrode as the working electrode, an Ag/AgCl (3.5 M KCl) reference and a platinum counter electrode. Fig. 3a shows the linear sweep voltammetry (LSV) curves of the $BiVO_4$ and $TiO_2/BiVO_4$ electrodes. In the dark those electrodes show little photocurrent density. However, in the light, the differences in the TiO_2 on the $BiVO_4$ electrode resulted in a different photocurrent density, and $TiO_2/BiVO_4$ electrodes had a significantly enhanced photocurrent density compared to $BiVO_4$ and TiO_2 electrodes. The 30 min-$TiO_2/BiVO_4$ electrode had the highest photocurrent density, with a value of 3.3 mA cm^{-2} at 1.23 V *vs.* RHE, which was 2.5 times that of $BiVO_4$. However, the 60 min-$TiO_2/BiVO_4$ electrode had lower photocurrent density compared to 30 min-$TiO_2/BiVO_4$, which may be a result of TiO_2 hindering charge transfer. A significant cathodic shift of onset potential was observed. For the 30 min-$TiO_2/BiVO_4$ electrode, the potential at 0.5 mA cm^2 was reduced greater than 500 mV, indicating an efficient charge separation or charge transfer originating from the formation of a heterojunction.

To test the charge recombination behaviour of the $TiO_2/BiVO_4$ electrodes, 0.1 M Na_2SO_3 solution was added to the electrolyte as a hole scavenger for the PEC measurements. The LSV curves of $TiO_2/BiVO_4$ electrodes are shown in Fig. 3b. $TiO_2/$

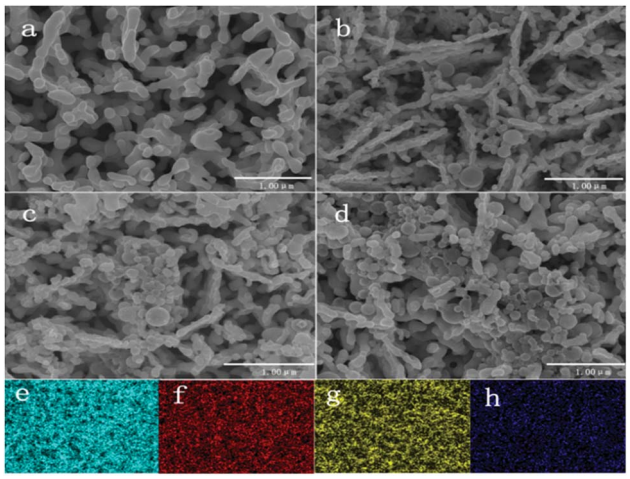

Fig. 1 SEMs of different electrodes. (a) $BiVO_4$, (b) 10 min-$TiO_2/BiVO_4$, (c) 30 min-$TiO_2/BiVO_4$, (d) 60 min-$TiO_2/BiVO_4$, and EDX-mapping of $TiO_2/BiVO_4$ are shown (e) Bi, (f) V, (g) O, (h) Ti.

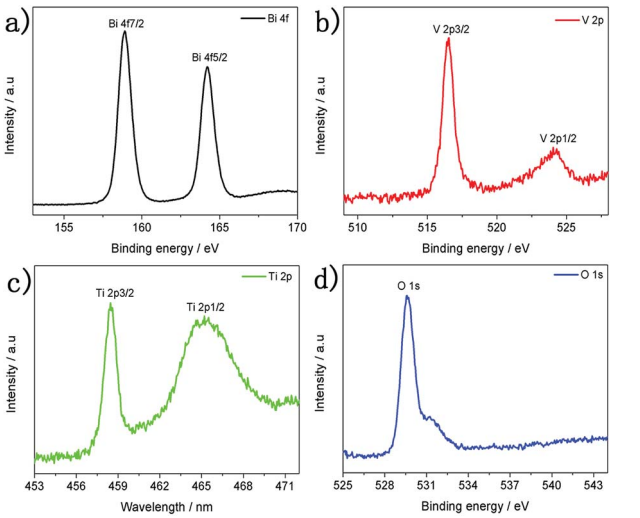

Fig. 2 XPS spectra of the $TiO_2/BiVO_4$ electrode (a) Bi 4f, (b) V 2p, (c) Ti 2p, (d) O 1s.

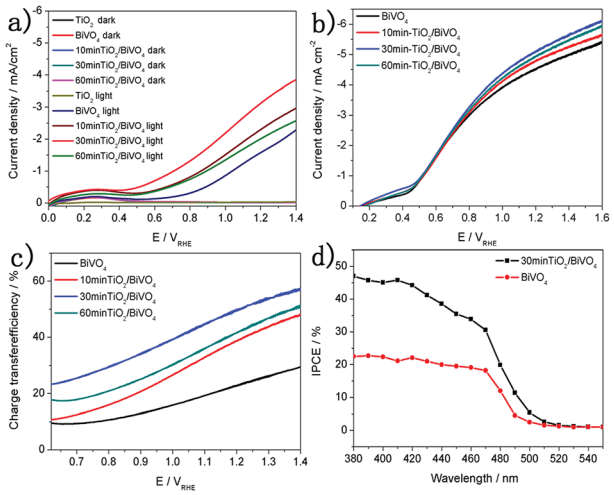

Fig. 3 (a) LSV curves of different $TiO_2/BiVO_4$ electrodes. (b) LSV of curves $BiVO_4$ and $TiO_2/BiVO_4$ in 0.1 M PBS containing 0.1 M Na_2SO_3. (c) The charge transfer efficiencies of different TiO_2 content on $BiVO_4$. (d) IPCEs of $BiVO_4$ and $TiO_2/BiVO_4$ electrodes.

$BiVO_4$ electrodes show higher photocurrent density compared to the $BiVO_4$ electrode, demonstrating a heterojunction was formed and better charge separation occurred. The 30 min-$TiO_2/BiVO_4$ electrode had the highest photocurrent density, 5.4 mA cm^{-2} at 1.23 V *vs.* RHE. The photocurrent can be described as: $J = J_{abs} \times \eta_{sep} \times \eta_{tr}$[38] the η_r values can be calculated as $J_{water}/J_{Na_2SO_3}$. As shown in Fig. 3c, all $TiO_2/BiVO_4$ electrodes had improved η_{tr} compared to the $BiVO_4$ electrode, over the range tested in this study. The 30 min-$TiO_2/BiVO_4$ electrode had the highest η_{tr}, 60% at 1.23 V *vs.* RHE, 3 times that of the $BiVO_4$ electrode. These results demonstrate that the construction of a $TiO_2/BiVO_4$ heterojunction could promote charge separation and charge transfer efficiencies. The incident-photon-to-current-conversion efficiency (IPCE) values are shown in Fig. 3d. The $TiO_2/BiVO_4$ was higher than $BiVO_4$ across the visible spectrum and at 520 nm the two electrodes reached 0, which is in agreement with the light absorbance of $BiVO_4$ and $TiO_2/BiVO_4$ electrodes (Fig S6†).

The photocurrent transient behaviours of the $TiO_2/BiVO_4$ electrodes were measured in 0.1 M PBS. A photocurrent spike was obtained using sudden illumination due to capacitive charging of the interface, and the spike decay due to the recombination of the electrons and holes that is associated with holes getting trapped at the electrode surface. A stabilised photocurrent was achieved when the charge generation and recombination rates were equal. Furthermore, the recombination rate could be reflected by longer transient decay times, which can be analysed on a logarithmic plot of parameter D, using the following equation:[39]

$$D = (I_t - I_s)/(I_m - I_s)$$

where: I_t is the photocurrent density at time t, I_s is the stabilised photocurrent density and I_m is the photocurrent density spike. The transient decay time can be defined as the time at which $\ln D = -1$. Fig. 4a shows the logarithmic plots of parameter D of the $BiVO_4$ and $TiO_2/BiVO_4$ electrodes. The transient decay time for $TiO_2/BiVO_4$ was 4.1 s, longer than that of $BiVO_4$ (1.5 s), suggesting a lower rate of electron and hole recombination in $TiO_2/BiVO_4$, which could be attributed to the TiO_2 nanospheres acting as hole resistors, resulting in increased efficiency of charge separation and prolonging the lifetime of the holes. As a result, abundant photogenerated charge carriers in the $TiO_2/BiVO_4$ electrode were effectively collected, leading to an improved PEC performance.

To characterise the kinetics of the charge transfer process of the $TiO_2/BiVO_4$ and $BiVO_4$ electrodes, electrochemical impedance spectroscopy (EIS) tests were performed at 1.23 V *vs.* RHE in 0.1 M PBS under simulated solar light illumination. Fig. 4b shows Nyquist at frequencies from 1 Hz to 100 kHz. The BiVO4 electrode had the greatest resistance to charge transfer and the 30 min-$TiO_2/BiVO_4$ had the lowest charge transfer resistance. However, the 60 min-$TiO_2/BiVO_4$ electrode had a lower charge transfer resistance, which may be a result of the TiO_2 impeding the transfer of surface charge, further indicating the optimum amount of TiO_2 was achieved in the 30 min-$TiO_2/BiVO_4$ electrode. The above results suggest that the TiO_2 facilitates the $BiVO_4$ electrode charge separation and transfer.

In order to further investigate the PEC performance, a molecular Co–cubane water oxidation catalyst was immobilised onto the $TiO_2/BiVO_4$ electrode. As the LSV curves show in Fig. 5a, the Co–cubane/$TiO_2/BiVO_4$ photoanode exhibits a high photocurrent density of 4.6 mA cm^{-2} at 1.23 V *vs.* RHE, 3.1 times higher than that of $BiVO_4$, indicating that the Co–cubane was acting as an efficient OER catalyst, further enhancing the charge transfer. Furthermore, after 400 s photoelectrolysis, the photocurrent density of Co–cubane/$TiO_2/BiVO_4$ could maintain more than 2.6 mA cm^{-2}, which is 2.6 times than that of the bare $BiVO_4$ (Fig S7†). The half-cell photoconversion efficiencies of $BiVO_4$ and Co–cubane/$TiO_2/BiVO_4$ electrodes were calculated using the LSV results, (Fig. 5b). The maximum value of Co–cubane/$TiO_2/BiVO_4$ achieved 1.48% at 0.72 V, approximately 6 fold compared to $BiVO_4$. The XPS spectra of the Co–cubane/$TiO_2/BiVO_4$ electrode was shown in Fig S8,† which indicated the element of Co was exited.

To explore the charge transfer mechanism between the $BiVO_4$ and TiO_2, Mott–Schottky plots of the $BiVO_4$ and TiO_2 were performed under dark conditions.[40] In Fig S9b,† the linear part of Mott–Schottky plots of $TiO_2/BiVO_4$ rather than $BiVO_4$ show the gentlest slope and the more negative flatband potential. The gentle slope means the modifying with TiO_2 can obviously

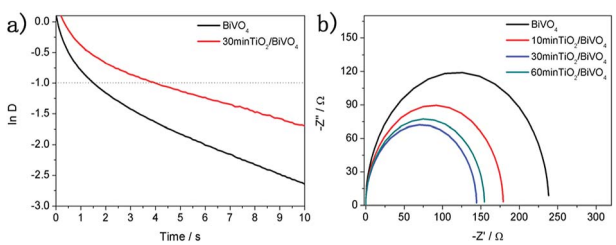

Fig. 4 (a) The logarithmic plots of the parameter D of the $BiVO_4$ and $TiO_2/BiVO_4$ electrodes. (b) Electrochemical impedance spectroscopy (EIS) of the TiO_2 under different soaking times.

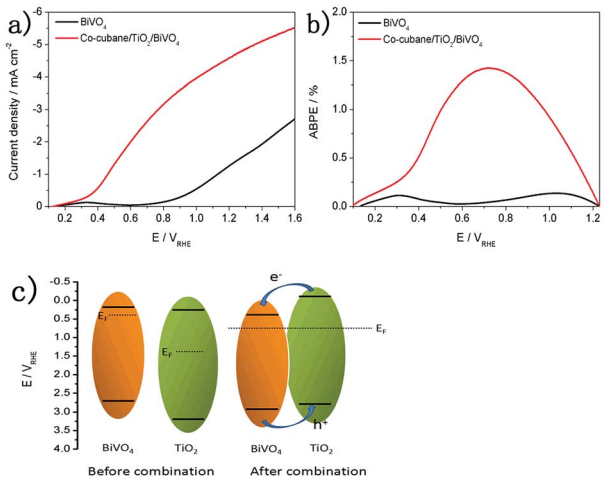

Fig. 5 (a) LSV curves of $BiVO_4$ and Co–cubane/TiO_2/$BiVO_4$ electrodes. (b) ABPEs of $BiVO_4$ and Co–cubane/TiO_2/$BiVO_4$ electrodes. (c) The charge transfer mechanism of TiO_2/$BiVO_4$ electrode.

increase the density of the carriers.[41] From Fig S9a and c,† the CB position of $BiVO_4$ and TiO_2 were 0.12 eV and 0.2 eV. And from Fig S10,† the band gap energies of $BiVO_4$ and TiO_2 were 2.42 eV and 3.09 eV. Therefore, the VB position of $BiVO_4$ and TiO_2 were 2.54 eV and 3.29 eV, calculated using $E_{CB} = E_{VB} - E_g$. Compared the $BiVO_4$, the TiO_2 approach to the intrinsic semiconductor, So we suppose the charge transfer mechanism shown the Fig. 5c, When these two types of semiconductor materials are closely joined together, the heterojunction structure was formed. At this moment, the two semiconductors have a uniform Fermi level and the system is in equilibrium. An electron transfer from TiO_2 to $BiVO_4$ possibly occurred, providing evidence for the efficient charge transfer between $BiVO_4$ and TiO_2.

Conclusions

In summary, a simple hydrothermal method was proposed to produce a TiO_2/$BiVO_4$ heterojunction electrode. The proposed TiO_2/$BiVO_4$ electrode provided a high performance for the oxidation of PEC water. The TiO_2/$BiVO_4$ heterojunction results indicate good charge separation and transfer efficiency. When a molecular Co–cubane catalyst was attached onto the TiO_2/$BiVO_4$ electrode, a further improvement in the PEC performance was achieved, with a photocurrent of photocurrent density of 4.6 mA cm^{-2} at 1.23 V, more than 3 times for $BiVO_4$ alone. This study provides a simple and effective approach in the production of heterojunction photoelectrodes for increasing the performance of PEC, which could be used to design efficient photocatalytic systems in future studies.

Conflicts of interest

The authors declare no conflict of interest.

Acknowledgements

This work was supported by the National Natural Science Foundation of China (21401092, 21671089, 21773100), the Shenyang Natural Science Foundation of China (F16-103-4-00), Scientific Research Found of Liaoning Province (LT2017010, 20170540409, 20180510011).

References

1 A. Kudo and Y. Miseki, *Chem. Soc. Rev.*, 2009, **38**, 253–278.
2 O. Khaselev, *Science*, 1998, **280**, 425–427.
3 Z. Li, W. Luo, M. Zhang, J. Feng and Z. Zou, *Energy Environ. Sci.*, 2013, **6**, 347–370.
4 M. Grätzel, *Nature*, 2001, **414**, 338–344.
5 K. O. Akihiko Kudo and H. Kato, *J. Am. Chem. Soc.*, 1999, **121**, 11459–11467.
6 F. E. Osterloh, *Chem. Soc. Rev.*, 2013, **42**, 2294–2320.
7 Z. Yin, Z. Wang, Y. Du, X. Qi, Y. Huang, C. Xue and H. Zhang, *Adv. Mater.*, 2012, **24**, 5374–5378.
8 H. K. Saimi Tokunaga and A. Kudo, *Chem. Mater.*, 2001, **13**, 4624–4628.
9 M. Zhong, T. Hisatomi, T. Minegishi, H. Nishiyama, M. Katayama, T. Yamada and K. Domen, *J. Master. Chem. A*, 2016, **4**, 9858–9864.
10 T. W. Kim and K. S. Choi, *Science*, 2014, **343**, 990–994.
11 G. Wang, Y. Ling, X. Lu, F. Qian, Y. Tong, J. Z. Zhang, V. Lordi, C. Rocha Leao and Y. Li, *J. Phys. Chem. C*, 2013, **117**, 10957–10964.
12 Y. Park, D. Kang and K. S. Choi, *Phys. Chem. Chem. Phys.*, 2014, **16**, 1238–1246.
13 M. Huang, J. Bian, W. Xiong, C. Huang and R. Zhang, *J. Master. Chem. A*, 2018, **6**, 3602–3609.
14 B. Klahr, S. Gimenez, F. Fabregat-Santiago, J. Bisquert and T. W. Hamann, *J. Am. Chem. Soc.*, 2012, **134**, 16693–16700.
15 C. Zachaus, F. F. Abdi, L. M. Peter and R. van de Krol, *Chem. Sci.*, 2017, **8**, 3712–3719.
16 F. F. Abdi and R. van de Krol, *J. Phys. Chem. C*, 2012, **116**, 9398–9404.
17 B. Zhang, L. Wang, Y. Zhang, Y. Ding and Y. Bi, *Angew. Chem., Int. Ed. Engl.*, 2018, **57**, 2248–2252.
18 H. Zhang, Y. Yu, L. Zhang and S. Dong, *Angew. Chem., Int. Ed. Engl.*, 2018, **57**, 1547–1551.
19 S. Gu, W. Li, F. Wang, S. Wang, H. Zhou and H. Li, *Appl. Catal., B*, 2015, **170–171**, 186–194.
20 A. P. Singh, N. Kodan, B. R. Mehta, A. Held, L. Mayrhofer and M. Moseler, *ACS Catal.*, 2016, **6**, 5311–5318.
21 S.-W. Cao, Z. Yin, J. Barber, F. Y. C. Boey, S. C. J. Loo and C. Xue, *ACS Appl. Mater. Interfaces*, 2011, **4**, 418–423.
22 L. Zhang, L. O. Herrmann and J. J. Baumberg, *Sci. Rep.*, 2015, **5**, 16660.
23 H. Hirakawa, S. Shiota, Y. Shiraishi, H. Sakamoto, S. Ichikawa and T. Hirai, *ACS Catal.*, 2016, **6**, 4976–4982.
24 J. Su, L. Guo, N. Bao and C. A. Grimes, *Nano Lett.*, 2011, **11**, 1928–1933.
25 P. Chatchai, Y. Murakami, S.-y. Kishioka, A. Y. Nosaka and Y. Nosaka, *Electrochim. Acta*, 2009, **54**, 1147–1152.

26 Y. Pihosh, I. Turkevych, K. Mawatari, T. Asai, T. Hisatomi, J. Uemura, M. Tosa, K. Shimamura, J. Kubota, K. Domen and T. Kitamori, *Small*, 2014, **10**, 3692–3699.
27 S. Ho-Kimura, S. J. A. Moniz, A. D. Handoko and J. Tang, *J. Master. Chem. A*, 2014, **2**, 3948–3953.
28 H. Zhang and C. Cheng, *ACS Energy Lett.*, 2017, **2**, 813–821.
29 M. Xie, X. Fu, L. Jing, P. Luan, Y. Feng and H. Fu, *Adv. Energy Mater.*, 2014, **4**, 1300995.
30 J. S. Yang, W. P. Liao and J. J. Wu, *ACS Appl. Mater. Interfaces*, 2013, **5**, 7425–7431.
31 Y. Ma, X. Wang, Y. Jia, X. Chen, H. Han and C. Li, *Chem. Rev.*, 2014, **114**, 9987–10043.
32 D. Lee, A. Kvit and K.-S. Choi, *Chem. Mater.*, 2018, **30**, 4704–4712.
33 S. S. Kalanur, I.-H. Yoo, J. Park and H. Seo, *J. Master. Chem. A*, 2017, **5**, 1455–1461.
34 L. Dong, S. Guo, S. Zhu, D. Xu, L. Zhang, M. Huo and X. Yang, *Catal. Commun.*, 2011, **16**, 250–254.
35 Y. Guo, X. Yang, F. Ma, K. Li, L. Xu, X. Yuan and Y. Guo, *Appl. Surf. Sci.*, 2010, **256**, 2215–2222.
36 N. Myung, S. Ham, S. Choi, Y. Chae, W.-G. Kim, Y. J. Jeon, K.-J. Paeng, W. Chanmanee, N. R. de Tacconi and K. Rajeshwar, *J. Phys. Chem. C*, 2011, **115**, 7793–7800.
37 N. J. Bell, Y. H. Ng, A. Du, H. Coster, S. C. Smith and R. Amal, *J. Phys. Chem. C*, 2011, **115**, 6004–6009.
38 D. K. Zhong, S. Choi and D. R. Gamelin, *J. Am. Chem. Soc.*, 2011, **133**, 18370–18377.
39 A. L. Hagfeldt, H. Lindström, S. Soedergren and S.-E. Lindquist, *J. Electroanal. Chem.*, 1995, **381**, 39–46.
40 J. A. T. G. Cooper and A. J. Nozik, *J. Electrochem. Soc.*, 1982, **129**, 1973–1977.
41 F. Ning, M. Shao, S. Xu, Y. Fu, R. Zhang, M. Wei, D. G. Evans and X. Duan, *Energy Environ. Sci.*, 2016, **9**, 2633.